Received: 29 June 2020 | Revised: 9 September 2020 | Accepted: 6 October 2020

DOI: 10.1002/mrc.5107

RESEARCH ARTICLE

WILEY

A structural analysis of 2,5-diaryl-4*H*-2,4-dihydro-3*H*-1,2,4-triazol-3-ones: NMR in the solid state, X-ray crystallography, and GIPAW calculations

Marta Marín-Luna[1] | **Pilar Sánchez-Andrada**[1] | **Ibon Alkorta**[2] | **José Elguero**[2] | **M. Carmen Torralba**[3] | **Patricia Delgado-Martínez**[4] | **Dolores Santa María**[5] | **Rosa M. Claramunt**[5]

[1]Departamento de Química Orgánica, Facultad de Química, Universidad de Murcia, Regional Campus of International Excellence "Campus Mare Nostrum", Murcia, Spain

[2]Instituto de Química Médica, CSIC, Madrid, Spain

[3]Departamento de Química Inorgánica, Facultad de Ciencias Químicas, UCM, Madrid, Spain

[4]Unidad de Difracción de Rayos X - CAI técnicas físicas y químicas, Facultad de Ciencias Químicas, UCM, Madrid, Spain

[5]Departamento de Química Orgánica y Bio-Orgánica, Facultad de Ciencias, UNED, Madrid, Spain

Correspondence
Marta Marín-Luna, Departamento de Química Orgánica, Facultad de Química, Universidad de Murcia, Murcia E-30100, Spain.
Email: martamarin@um.es

Funding information
Fundación Seneca-CARM, Grant/Award Number: 20811/PI/18; Comunidad de Madrid, Grant/Award Number: P2018/EMT-4329 AIRTEC-CM; Spanish MICINN, Grant/Award Numbers: CTQ2017-87231-P, CTQ2018-094644-B-C22

Abstract

The ^{1}H, ^{13}C, ^{15}N, and ^{19}F nuclear magnetic resonance (NMR) spectra of 11 2,5-diaryl-2,4-dihydro-3*H*-1,2,4-triazol-3-ones have been acquired in DMSO-d_6 solution and the ^{13}C, ^{15}N, and ^{19}F NMR spectra have also been acquired in the solid state (solid-state nuclear magnetic resonance [SSNMR] and magic angle spinning [MAS]). The X-ray structures of Compounds **3**, **5**, and **6** have been determined by X-ray diffraction. Theoretical calculations at the gauge-independent atomic orbital (GIAO)/B3LYP/6-311++G(d,p) level have provided a set of 321 chemical shifts that were compared with 310 experimental values in DMSO-d_6. To obtain good agreements, some effects need to be included. The SSNMR chemical shifts have been compared with gauge-including projector-augmented wave (GIPAW) calculations and with the heavy atom–light atom (HALA) effects.

KEYWORDS

1,2,4-triazol-3-ones, GIPAW, hydrogen bonds, SSNMR

1 | INTRODUCTION

We recently reported the pharmacological activity of 10 2,5-diaryl-1,2,4-triazol-3-ones (**1**–**10**)[1] (Figure 1) towards several relevant cancer targets. Some showed relatively high activities together with poor toxicity in non-tumor cell lines. 2-(2-Fluorophenyl)-5-(3-methoxyphenyl)-2,4-dihydro-3*H*-1,2,4-triazol-3-one (**2**) was particularly active regarding *c-Myc* and *PD-L1* gene expression, whereas 2-(4-chloro-2-fluorophenyl)-5-(3-methoxyphenyl)-2,4-dihydro-3*H*-1,2,4-triazol-3-one (**6**) is the one that combined the best down-regulatory activities in three genes.

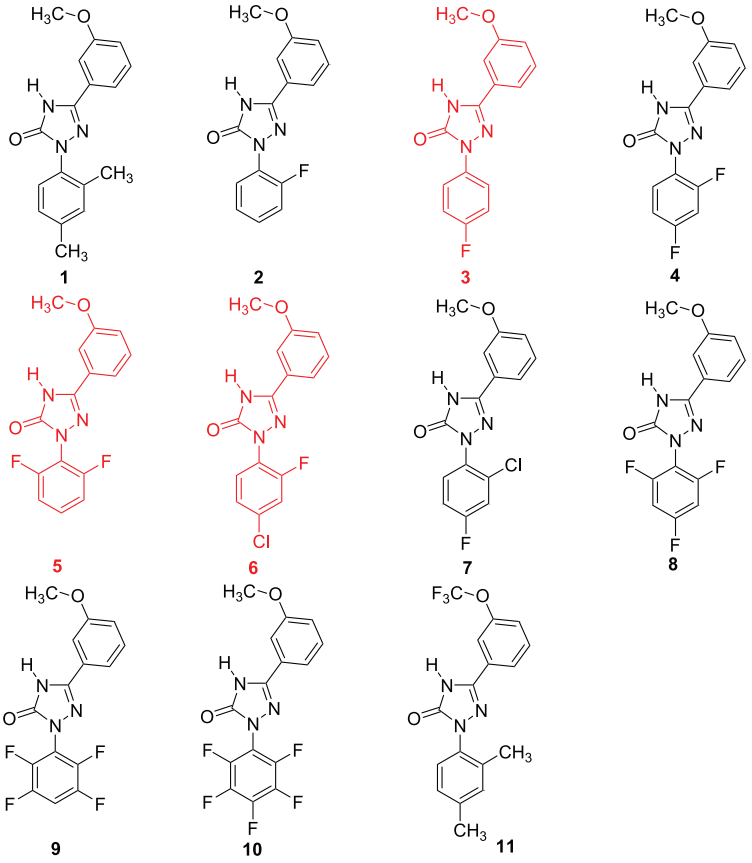

FIGURE 1 Structures of the 11 2,5-diaryl-2,4-dihydro-3*H*-1,2,4-triazol-3-ones studied in this work. The structures highlighted in red were those determined by X-ray crystallography

Concerning protein expression, the most active compounds were **3** and **8** (*c-Myc* expression) and **9** (*PD-L1* expression).

Due to its biological properties, many other triazol-3-ones, not necessarily having a 2,5-diaryl pattern, have previously been described; they are Ca^{2+} conductance openers activated potassium channels,[2] antimicrobials,[3] antifungals,[4,5] TNF-α inhibitors,[6] selective CB1 receptor antagonists,[7] angiotensin II AT1 receptor antagonists,[8,9] antioxidants,[10] and AChE inhibitors.[11]

A thorough understanding of biological properties requires information about the structure of molecules, among them tautomerism[1] and conformational isomerism. Conformational data are usually obtained in solution by nuclear magnetic resonance (NMR)[12,13] and quantum chemical calculations[14,15] and in the solid-state by NMR,[16,17] crystallography,[18,19] and again by quantum calculations.[20,21]

In our previous paper,[1] the NMR data of these compounds were determined in solution and reported in the experimental section without comments. We elected to pursue a more detailed discussion of compounds previously reported[1] with the following differences:

- Solution data have been reported in detail.
- Solid-state NMR (SSNMR) spectra have been measured for the first time.
- The structures of three compounds (**3**, **5**, and **6**) have been confirmed by X-ray.
- Theoretical calculations of the chemical shifts for both solution (gauge-independent atomic orbital [GIAO]) and solid state (gauge-including projector-augmented wave [GIPAW]) have been carried out.
- Compound **11** having a trifluoromethoxy group instead of a methoxy group was prepared to understand the effect of the alkoxy groups on the conformational isomerism.

TABLE 1 Hydrogen bonds (bond distances in Å and angles in °) for Compounds **3**, **5**, and **6**

Comp.	D–H···A	Symmetry operations	d(D–H)	d(H···A)	d(D···A)	<(DHA)
3	N4–H4···O1	1–*x*,2–*y*,1–*z*	1.02(5)	1.77(5)	2.777(4)	173(4)
5	N4A–H4A···O1B		0.88(2)	1.84(2)	2.712(2)	172(2)
	N4B–H4B···O1A		0.88(2)	1.93(2)	2.800(2)	170(2)
6	N4–H4···O1	1–*x*,1–*y*,1–*z*	0.86	1.96	2.817(3)	171.8

TABLE 2 ^{1}H NMR chemical shifts (δ, ppm) and ^{1}H–^{1}H coupling constants (Hz) in DMSO-d_6

Comp.	N–H	H-2′ CH_3	H-3′	H-4′ CH_3	H-5′
1	12.40 (br s)	2.19 (s)	7.16 (br s)	2.32 (s)	7.10 (br d)
2	12.56 (br s)	---	7.42 (m)	7.48 (dddd) ^{3}J(H5′) = 8.4 ^{3}J (H3′) = 7.3 ^{4}J(F) = 5.1 ^{4}J (H6′) = 1.7	7.34 (ddd) ^{3}J(H4′) = 8.4 ^{3}J (H6′) = 7.7 ^{4}J (H3′) = 1.4
3	12.62 (br s)	7.99 (m) ^{3}J(H3′) = 9.0 ^{4}J(F) = 5.0 ^{4}J (H6′) = 2.8	7.31 (m) ^{3}J(H2′) = 9.0 ^{3}J (F) = 9.0 ^{4}J(H5′) = 3.0	---	7.31 (m) ^{3}J(H2′) = 9.0 ^{3}J (F) = 9.0 ^{4}J(H5′) = 3.0
4	12.57 (br s)	---	7.50 (ddd) ^{3}J(F2′) = 10.6 ^{4}J (F4′) = 9.0 ^{4}J(H5′) = 2.8	---	7.24 (dddd) ^{3}J(H6′) = 8.8 ^{3}J(F4′) = 8.8 ^{4}J(H3′) = 2.8 ^{5}J(F2′) = 1.4
5	12.68 (br s)	---	7.35 (br dd)	7.63 (dddd) ^{3}J(H5′) = 8.5 ^{3}J (H3′) = 8.5 ^{4}J(F2′) = 6.4 ^{4}J (F6′) = 6.4	7.35 (br dd)
6	12.59 (br s)	---	7.68 (dd) ^{3}J(F) = 10.3 ^{4}J (H5′) = 2.1	---	7.43 (m)
7	12.52 (br s)	---	7.69 (dd) ^{3}J(F) = 8.5 ^{4}J (H5′) = 2.8	---	7.39 (m)
8	12.71 (br s)	---	7.50 (ddd) ^{3}J(F2′) = 10.9 ^{3}J(F4′) = 8.4 ^{5}J (F6′) = 3.1	---	7.50 (ddd) ^{3}J(F6′) = 10.9 ^{3}J(F4′) = 8.4 ^{5}J (F2′) = 3.1
9	12.86 (br s)	---	---	8.14 (dddd) ^{3}J(F3′) = 10.8 ^{3}J (F5′) = 10.8 ^{4}J(F2′) = 7.5 ^{4}J (F6′) = 7.5	---
10	12.88 (br s)	---	---	---	---
11	12.51 (br s)	2.19 (s)	7.17 (s)	2.32 (s)	7.11 (d) ^{3}J(H6′) = 8.0

Comp.	H-6′	H-2″	OCH_3	H-4″	H–5″	H-6″
1	7.24 (d) ^{3}J(H5′) = 7.8	7.39 (m)	3.80 (s)	7.05 (m)	7.41 (m)	7.40
2	7.61 (ddd) ^{3}J(H5′) = 7.7 ^{3}J(F) = 7.7 ^{4}J (H4′) = 1.7	7.40 (m)	3.80 (s)	7.07 (m)	7.42 (m)	7.42 (m)
3	7.99 (m) ^{3}J(H3′) = 9.0 ^{4}J(F) = 5.0 ^{4}J (H6′) = 2.8	7.45 (m)	3.82 (s)	7.09 (ddd) ^{3}J(H5″) = 8.0 ^{4}J(H2″) = 2.5 ^{4}J (H6″) = 1.2	7.44 (dd) ^{3}J (H4″) = 8.0 ^{3}J (H6″) = 7.8	7.49 (ddd) ^{3}J(H5″) = 7.8 ^{4}J(H2″) = 2.5 ^{4}J (H4″) = 1.2
4	7.68 (ddd) ^{3}J(H5′) = 8.8 ^{4}J(F2) = 8.8 ^{4}J (F4) = 6.0	7.39 (m)	3.80 (s)	7.07 (m)	7.42 (m)	7.42 (m)
5	---	7.39 (br dd)	3.80 (s)	7.08 (m)	7.43 (m)	7.43 (m)
6	7.67 (dd) ^{3}J(H5′) = 8.4 ^{4}J(F) = 8.4	7.40 (m)	3.80 (s)	7.08 (m)	7.43 (m)	7.43 (m)
7	7.70 (dd) ^{3}J(H5′) = 8.9 ^{4}J(F) = 5.7	7.39 (m)	3.80 (s)	7.07 (m)	7.41 (m)	7.42 (m)
8	---	7.39 (m)	3.80 (s)	7.09 (m)	7.42 (m)	7.42 (m)
9	---	7.40 (m)	3.81 (s)	7.11 (m)	7.44 (m)	7.44 (m)

(Continues)

TABLE 2 (Continued)

Comp.	H-6′	H-2″	OCH_3	H-4″	H–5″	H-6″
10	---	7.39 (m)	3.80 (s)	7.11 (m)	7.45 (m)	7.43(m)
11	7.25 (d) ^3J(H5′) = 8.0	7.79 (br s)	---	7.49 (d) ^3J(H5″) = 8.0	7.65 (dd) ^3J (H4″) = 8.0 ^3J (H6″) = 8.0	7.87 (d) ^3J(H5″) = 8.0

Abbreviation: ^{1}H NMR, hydrogen-1 nuclear magnetic resonance.

- The compounds under study are represented in Figure 1; the compounds depicted in red are the three structures that have been confirmed by X-ray crystallography.

2 | RESULTS AND DISCUSSION

2.1 | General comments

We will report our results in the following order: Section 2.2, crystal structures including disorder (Table 1); Section 2.3, NMR results (Tables 2-8) including substituent and phase effects (gas, DMSO, and solid state); Section 2.4, conformational studies divided, in turn, into solution (energies and chemical shifts) and solid state, to end up with experimental details and conclusions.

2.2 | Crystal structures

Suitable crystals of Compounds **3**, **5**, and **6** for single X-ray diffraction were obtained as follows: Compound **3** from DMSO–water and Compounds **5** and **6** from DMSO. 2-(4-Fluorophenyl)-5-(3-methoxyphenyl)-2,-4-dihydro-3*H*-1,2,4-triazol-3-one (**3**) and 2-(4-chloro-2-fluorophenyl)-5-(3-methoxyphenyl)-2,4-dihydro-3*H*-1,2,4-triazol-3-one (**6**) crystallize in the monoclinic $P2_1/n$ and triclinic *P*-1 space groups, respectively, with one molecule in their asymmetric units. 2-(2,6-Difluorophenyl)-5-(3-methoxyphenyl)-2,4-dihydro-3*H*-1,2,4-triazol-3-one (**5**) crystallizes in the orthorhombic *Pbca* space group, with two crystallographically independent molecules A and B in the asymmetric unit that arrange the triazolone rings in an alternated disposition. Oak Ridge Thermal Ellipsoid Plots (ORTEPs) of all structures are depicted in Figure S1.

All three compounds form dimeric units between neighboring molecules (Figure 2) as expected and the distances and angles of the hydrogen bonds (HBs) for these compounds are summarized in Table 1. The dimers arrange by a hydrogen bonding interaction between the carbonyl and the N4H4 groups of the triazolone (O1···H4–N4) of two opposite molecules. The double interaction is symmetrical for **3** and **6** with a distance O1···H4–N4 of 1.77(5) and 1.96 Å, respectively (Table 1). However, **5** forms dimers by contacts between A and B type molecules giving rise to asymmetrical HBs with distances O1B···H4A–N4A of 1.84(2) Å and O1A··· H4B–N4B of 1.93(2) Å.

The presence of different substituents on the N2 atom of the triazolone does not exert a significant influence on the bond distances in that ring, as they are quite similar in the three compounds. Nevertheless, the strength of the HBs in the dimers could relate to the presence of the different substituents on the aryl rings and, therefore, the resulting molecular shape.

Comparing the data, a higher molecular distortion agrees with poorer hydrogen bonding interactions in the dimeric unit arrangement. In such context, the molecules in Compound **3** are completely planar due to the coplanar arrangement of the three rings, showing a greater hydrogen bonding interaction with the shortest bond distance (Table 1). However, the molecules in **6** keep only a partial planarity on the fragment formed by the triazolone and the 3-(methoxyphenyl) rings, but the other aromatic ring is clearly twisted (Figure 2). In that sense, the dihedral angle defined by the triazole and the 3-methoxyphenyl rings is 4.2(3)°, and the one for the triazole and the difluorophenyl rings is 37.7(3)°. The twisting of the molecules is related to the steric factors due to the presence of a fluorine substituent at the *ortho* position of the aromatic ring that introduces a higher steric hindrance compared with **3** in which the fluorine atom occupies the *para* position. Moreover, it is worth noting that the positional disorder of the fluorine in Compound **6** over the two *ortho* positions, modeled for occupancies of 80:20 ratio, which could influence the torsion of that ring. This fact becomes more evident in **5**, which has the two *ortho* positions substituted by fluorine atoms, showing values for the related dihedral angles of 4.3(3)° and 65.5(3)° for type A molecules and 12.4(3)° and 61.2(3)° for type B ones.

TABLE 3 ^{13}C NMR chemical shifts (δ, ppm) in DMSO-d_6; spin–spin ^{13}C–^{19}F coupling constants (Hz)

Comp.	CO	C-5	C-1′	C-2′	C-3′	C-4′	C-5′	C-6′
1	153.4	144.5	133.3	134.5	131.2	137.9	126.9[a]	127.0[a]
2	153.3	145.5	124.3 $^{2}J_{F} = 12.1$	156.1 $^{1}J_{F} = 251.0$	116.6 $^{2}J_{F} = 18.9$	130.1 $^{3}J_{F} = 7.5$	124.8 $^{4}J_{F} = 3.7$	128.2
3	152.8	144.7	134.2 $^{4}J_{F} = 2.5$	120.1 $^{3}J_{F} = 7.9$	115.7 $^{2}J_{F} = 22.5$	159.2 $^{1}J_{F} = 242.6$	115.7 $^{2}J_{F} = 22.5$	120.1
4	153.4	145.6	121.1 $^{2}J_{F} = 12.0$ $^{4}J_{F} = 3.7$	156.5 $^{1}J_{F} = 254.3$ $^{3}J_{F} = 13.2$	105.2 $^{2}J_{F4} = 27.2$ $^{2}J_{F2} = 23.9$	161.5 $^{1}J_{F} = 248.1$ $^{3}J_{F} = 11.5$	112.0 $^{2}J_{F} = 22.7$ $^{4}J_{F} = 3.7$	129.7 $^{3}J_{F4} = 10.2$ $^{3}J_{F2} = 1.6$
5	153.7	146.4	113.4 $^{2}J_{F2'} = 15.9$ $^{2}J_{F6'} = 15.9$	158.3 $^{1}J_{F} = 253.5$ $^{3}J_{F} = 4.2$	112.6 $^{2}J_{F} = 18.2$ $^{4}J_{F} = 4.6$	131.8 $^{3}J_{F2'} = 10.1$ $^{3}J_{F6'} = 10.1$	112.6 $^{2}J_{F} = 18.2$ $^{4}J_{F} = 4.6$	158.3 $^{1}J_{F} = 253.5$ $^{3}J_{F} = 4.2$
6	153.2	145.8	123.5 $^{2}J_{F} = 11.8$	155.8 $^{1}J_{F} = 255.4$	117.4 $^{2}J_{F} = 23.1$	133.2 $^{3}J_{F} = 9.8$	125.1 $^{4}J_{F} = 3.6$	129.0 $^{3}J_{F} = 0.9$
7	153.5	145.3	130.8	132.7	117.5 $^{2}J_{F} = 26.9$	161.7 $^{1}J_{F} = 250.0$	115.3 $^{2}J_{F} = 22.6$	131.7
8	153.7	146.5	110.5 $^{2}J_{F2'} = 16.5$ $^{2}J_{F6'} = 16.5$ $^{4}J_{F4'} = 5.1$	158.7 $^{1}J_{F} = 253.6$ $^{3}J_{F4'} = 16.1$ $^{3}J_{F6'} = 6.5$	101.8 $^{2}J_{F4'} = 27.8$ $^{2}J_{F2'} = 24.6$ $^{4}J_{F6'} = 3.1$	162.2 $^{1}J_{F} = 250.0$ $^{3}J_{F2'} = 15.4$ $^{3}J_{F6'} = 15.4$	101.8 $^{2}J_{F4'} = 27.8$ $^{2}J_{F2'} = 24.6$ $^{4}J_{F6'} = 3.1$	158.7 $^{1}J_{F} = 253.6$ $^{3}J_{F4'} = 16.1$ $^{3}J_{F6'} = 6.5$
9	153.2	147.3	115.9 $^{2}J_{F2'} = 13.8$ $^{2}J_{F6'} = 13.8$ $^{3}J_{F3'} = 3.2$ $^{3}J_{F5'} = 3.2$	142.6 $^{1}J_{F} = 252.7$ $^{2}J_{F3'} = 15.1$ $^{3}J_{F6'} = 4.0$ $^{4}J_{F5'} = 2.2$	145.6 $^{1}J_{F} = 246.3$ $^{2}J_{F2'} = 12.4$ $^{3}J_{F5'} = 12.4$ $^{4}J_{F6'} = 4.2$	107.8 $^{2}J_{F3'} = 23.6$ $^{2}J_{F5'} = 23.6$	145.6 $^{1}J_{F} = 246.3$ $^{2}J_{F2'} = 12.4$ $^{3}J_{F5'} = 12.4$ $^{4}J_{F6'} = 4.2$	142.6 $^{1}J_{F} = 252.7$ $^{2}J_{F3'} = 15.1$ $^{3}J_{F6'} = 4.0$ $^{4}J_{F5'} = 2.2$
10	153.2	147.4	111.4 $^{2}J_{F2'} = 14.2$ $^{2}J_{F6'} = 14.2$	143.3 $^{1}J_{F} = 249.9$ $^{2}J_{F3'} = 11.9$ $^{3}J_{F4'} = 7.9$ $^{3}J_{F6'} = 4.1$	137.6 $^{1}J_{F} = 252.5$ $^{2}J_{F2'} = 14.1$ $^{2}J_{F4'} = 14.1$	141.3 $^{1}J_{F} = 254.0$ $^{2}J_{F3'} = 13.3$ $^{2}J_{F5'} = 13.3$ $^{3}J_{F2'} = 4.4$ $^{3}J_{F6'} = 4.4$	137.6 $^{1}J_{F} = 252.5$ $^{2}J_{F2'} = 14.1$ $^{2}J_{F4'} = 14.1$	143.3 $^{1}J_{F} = 249.9$ $^{2}J_{F3'} = 11.9$ $^{3}J_{F4'} = 7.9$ $^{3}J_{F6'} = 4.1$
11	153.4	143.3	133.0	134.5	131.27[a]	138.0	126.97[a]	127.04[a]

Comp.	C-1″	C-2″	C-3″	C-4″	C-5″	C-6″	OCH_3, OCF_3	CH_3
1	127.8	110.2	159.6	116.2	130.2	117.2	55.3	17.6 (2′) 20.6 (4′)
2	127.5	110.2	159.6	116.4	130.2	117.3	55.3	---
3	127.3	110.5	159.6	116.5	130.3	117.5	55.3	---
4	127.4	110.2	159.6	116.5	130.2	117.4	55.3	---
5	127.2	110.2	159.6	116.7	130.3	117.4	55.3	---
6	127.3	110.3	159.6	116.5	130.3	117.4	55.3	---
7	127.5	110.2	159.6	116.5	130.3	117.4	55.3	---
8	127.1	110.2	159.6	116.8	130.3	117.4	55.3	---
9	127.0	110.4	159.6	117.0	130.3	117.6	55.3	---
10	126.9	110.4	159.6	117.0	130.3	117.6	55.3	---
11	128.7	117.3	148.7	122.6	131.3[a]	123.9	120.0 $^{1}J_{F} = 256.5$	17.6 (2′) 20.6 (4′)

Abbreviation: ^{13}C NMR, carbon-13 nuclear magnetic resonance.

[a]Can be permuted.

TABLE 4 ^{13}C NMR chemical shifts (δ, ppm) in the solid state (CPMAS)

Comp.	CO	C-5	C-1′	C-2′	C-3′	C-4′	C-5′	C-6′
1	155.8	144.2	131.7	133.0	128.4	136.7	125.3[a]	124.0[a]
2[b]	153.8	146.2	123.6	153.8	115.9–117.0	127.0–128.7	123.6	127.0–128.7
3	154.5	146.0	134.2	120.5	115.6	161.7	115.6	120.5
4	153.9	147.4	120.4	158.5	104.4	163.2	109.8	129.0
5	156.3	146.5	112.8	160.9	112.4	132.4	112.4	160.9
6	153.4	144.7	122.9	154.8	118.4	135.4	122.9	130.4
7	155.4	144.7	129.9	136.1	113.9	161.8	112.0	131.6
8	154.1	146.3	110.7	159.6[a]	101.7[a]	162.1	98.5[a]	155.9[a]
9	155.6	147.2	117.0	144.7	144.7	104.1	144.7	144.7
10	153.9	146.7	112.3	142.1	137.1	142.1	137.1	142.1
11	154.6	142.4	131.6	136.2	130.2	138.8	125.8[a]	127.8[a]

Comp.	C-1″	C-2″	C-3″	C-4″	C-5″	C-6″	OCH_3, OCF_3	CH_3
1	127.4	106.9	159.5	116.1	131.7	118.6	54.6	19.6 (2′), 21.7 (4′)
2	126.5	107.7	159.1	115.9	127.0–128.7	117.0	55.1	---
3	124.7	105.9	158.7	116.8	130.1	118.6	54.5	---
4	124.7	106.4	161.0	117.2	129.0	119.0	54.6	---
5	127.5	110.8	160.3	116.8	129.5	118.0	55.1	---
6	125.0	107.5	158.7	118.4	130.4	118.4	56.4	---
7	126.0	110.0	158.3	116.7	129.9	116.7	54.6	---
8	125.6	104.0	158.1	118.5	129.3	118.5	53.6	---
9	125.7	108.0	159.2	117.0	128.0	119.9	54.1	---
10	125.2	103.9	159.3	116.9, 118.5	130.5	121.8	54.9	---
11	128.5	118.3	148.6	121.7	130.2	123.9	121.7	15.8 (2′), 21.7 (4′)

Abbreviations: ^{13}C NMR, carbon-13 nuclear magnetic resonance; CPMAS, cross-polarization magic angle spinning.
[a]Can be permuted.
[b]In Compound **2**, there are several carbon atoms with two values separated by a dash; they correspond to the interval of broad signals.

TABLE 5 ^{15}N NMR chemical shifts (δ, ppm) in DMSO-d_6 and some ^{15}N–^{19}F SSCC

Comp.	N-1	N-2	N-4
1	−112.6	−202.5	−242.5
2	−114.6	n.o.	−242.5
3	n.o.	−200.9	−239.0
4	−114.7	n.o.	−242.5
5	−114.1	−222.4	−242.9
6	−115.6 $^4J_F = 2.7$	−211.6 $^3J_F = 2.6$	−242.4
7	−113.5	−207.2	−242.9
8	−114.4	−223.9	−242.9
9	n.o.	−223.2	−241.8
10	−116.1	−225.1	−242.9
11	−110.8	−201.3	−241.4

Abbreviations: ^{15}N NMR, nitrogen-15 nuclear magnetic resonance, n.o., not observed; SSCC, spin–spin coupling constants.

TABLE 6 ^{15}N NMR chemical shifts (δ, ppm) in the solid state (CPMAS)

Comp.	N-1	N-2	N-4
1	−111.6	−197.6	−240.3
2	−113.7	−204.7	−240.6
3	−126.5	−198.2	−237.5
4	−116.4	−208.0	−240.9
5	−108.8, −112.9	−219.0	−240.2
6	−111.8	−204.0	−239.6
7	−110.3	−202.6	−240.4
8	−115.2	−216.4	−239.8
9	−114.6	−222.3	−241.9
10	−112.0	−217.9	−240.4, −242.5
11	−105.2	−195.7	−238.3

Abbreviations: ^{15}N NMR, nitrogen-15 nuclear magnetic resonance; CPMAS, cross-polarization magic angle spinning.

TABLE 7 ^{19}F NMR chemical shifts (δ, ppm) in DMSO-d_6; spin–spin ^{1}H–^{19}F coupling constants (Hz)

Comp.	F-2′/(F-6′)	F-3′/(F-5′)	F-4′	OCF_3
2	−120.4 (ddd) ^{3}J (H3′) = 10.7 ^{4}J (H6′) = 7.6 ^{4}J (H4′) = 5.1	---	---	---
3	---	---	−117.5 (dddd) ^{3}J (H3′) = 9.0 ^{3}J (H5′) = 9.0 ^{4}J (H2′) = 4.5 ^{4}J (H6′) = 4.5	---
4	−115.5 (dddd) ^{3}J (H3′) = 10.6 ^{4}J (H6′) = 8.8 ^{4}J (F4) = 7.8 ^{5}J (H5′) = 1.4	---	−108.9(dddd) ^{3}J (H3′) = 9.0 ^{3}J (H5′) = 8.8 ^{4}J (F2) = 7.8 ^{4}J (H6′) = 6.1	---
5	−118.3 (dd) ^{3}J (H3′) = 7.2 ^{4}J (H4′) = 7.2	---	---	---
6	−116.8 (ddd) ^{3}J (H3′) = 10.3 ^{4}J (H6′) = 8.4 ^{5}J (H5′) = 1.1	---	---	---
7	---	---	−109.7 (ddd) ^{3}J (H3′) = 8.4 ^{3}J (H5′) = 8.4 ^{4}J (H6′) = 5.8	---
8	−115.5 (d) ^{4}J (F4) = 7.1	---	−104.9 (dd) ^{4}J (F2) = 7.1 ^{4}J (F6) = 7.1	---
9	−145.4 (m)	−138.4 (m)	----	---
10	−145.4 (m)	−161.6 (m)	−152.5 (dd) ^{3}J (F3) = 22.7 ^{3}J (F5) = 22.7	---
11	---	---	---	−56.8 (s)

Abbreviation: ^{19}F NMR, fluorine-19 nuclear magnetic resonance.

Additionally, diverse steric hindrance in the three compounds also affects to the arrangement of the methoxy groups on the aromatic ring. In this way, in Compounds **3** and **6**, the methoxy groups are arranged pointing inwards the dimeric unit (on the same side of the N4H4) whereas in Compound **5**, which shows a greater molecular distortion, has the methoxy group points outwards away from the dimer on the same side of the N1 group (Figure 2).

Crystal packing effects for the three compounds are quite different depending on the directing forces involved in the supramolecular organization. Compound **3** forms a 2-D network due to weak F···H contacts among dimers (the F1···H15 distance is 2.582(4) Å) in which each dimer interacts with four adjacent ones, as shown in Figure 3. In **6** (Figure 4), however, only weak F···F contacts are observed leading to the formation of chains along *c* axis (the F1···F1 distance is 2.816(3) Å). In contrast, derivative **5** does not form an extended network becuase the weak F···H interactions between type A molecules of two different dimers (the F2A···H16A distance is 2.616(3) Å) along with a partial π–π overlapping of the methoxyphenyl rings (the shortest distance C···C about 3.3 Å) lead to the formation of tetrameric units. No significant contacts between these tetramers have been observed (Figure 5).

2.3 | NMR results

The ^{1}H, ^{13}C, ^{15}N, and ^{19}F NMR data of the Compounds **1–11** in DMSO-d_6 solution and in solid state are gathered in Tables 2–8. The ^{13}C shifts in the solid state were assigned by analogy to the solution-state

TABLE 8 ^{19}F NMR chemical shifts (δ, ppm) in the solid state (MAS)

Comp.	F-2′/(F-6′)	F-3′/(F-5′)	F-4′	OCF_3
2	−112.7	---	---	---
3	---	---	−112.6[a]	---
4	−106.8[b]	---	−105.2[b]	---
5	−113.6, −115.7	---	---	---
6	−107.6	---	---	---
7	---	---	−112.2	---
8	−108.9[a], −112.6	---	−106.9[a]	---
9	−144.1	−136.3	---	---
10	−138.4, −143.2	−161.6	−155.1	---
11	---	---	---	−54.5

Abbreviations: ^{19}F NMR, fluorine-19 nuclear magnetic resonance; MAS, magic angle spinning.

[a]A small broad singlet appears at −120.0 ppm that is not an impurity (absent in solution).

[b]Can be permuted.

experiments taking into account what DMSO is likely to do, being aware that solution and solid-state shifts can differ.

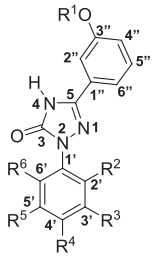

	R[1]	R[2]	R[3]	R[4]	R[5]	R[6]
1	CH_3	CH_3	H	CH_3	H	H
2	CH_3	F	H	H	H	H
3	CH_3	H	H	F	H	H
4	CH_3	F	H	F	H	H
5	CH_3	F	H	H	H	F
6	CH_3	F	H	Cl	H	H
7	CH_3	Cl	H	F	H	H
8	CH_3	F	H	F	H	F
9	CH_3	F	F	H	F	F
10	CH_3	F	F	F	F	F
11	CF_3	CH_3	H	CH_3	H	H

^{1}H, ^{13}C, ^{15}N, and ^{19}F NMR spectroscopy was used for the structural characterization of Compounds **1**–**11**. A complete set of chemical shifts and spin–spin coupling constants (SSCC) data in DMSO-d_6 is given in Tables 2, 3, 5, and 7, and are consistent with the assignments as well as with the cross peaks observed in the correlation spectroscopy (COSY), gradient-selected-heteronuclear single quantum correlation (gs-HMQC) (^{1}H–^{13}C), and gs-heteronuclear multiple bond correlation (HMBC) (^{1}H–^{13}C) experiments. *J*(H–F) SSCC were measured in the proton spectra, but when the signals of several protons overlapped, the values were obtained from the ^{19}F NMR spectra. *J*(F–F) SSCC were measured from the proton-decoupled ^{19}F NMR spectra. *J*(C–F) SSCC were directly obtained from the proton decoupled ^{13}C NMR spectra. In some compounds, *J*(F–N) coupling constants have been measured.

As we have already pointed out,[1] Compounds **1**–**10** exist as 4*H*-triazolones and not as hydroxytriazoles or 1*H*-triazolones tautomers,[22,23] which is consistent with the presence of a N4–H group that appears in the ^{1}H NMR spectra as a broad signal between 12.40 (**1**) and 12.88 ppm (**10**) and in ^{15}N NMR at around −242 ppm. The N2-aryl signals were observed in the range of −200.9 (**3**) (note that in **1** appears at −202.5 being the second smaller) to −225.1 ppm (**10**) and the N1 signal between −112.6 (**1**) and −116.1 ppm (**10**).[24]

The ^{13}C NMR signal of the CO groups appears at about 153 ppm and has been unambiguously identified as it does not present correlations with protons in the gs-HMBC (^{1}H–^{13}C) experiments, contrary to C3″ appearing in the same region, which shows cross peaks with the corresponding protons. Finally, the C5 carbon atom of the triazolone ring has been assigned taking into account that in the gs-HMBC (^{1}H–^{13}C) spectra, it must give cross peaks with the protons connected at three bonds (H2″ and H6″): It is the signal observed in the spectral region of 144.5 (**1**) to 147.4 ppm (**10**).

With one exception, the extreme ranges correspond to the 2,4-dimethylated **1** and to the pentafluorophenyl **10** N2-substituents; that is, the signal became more deshielded (higher frequency) as the number of fluorine atoms increases (**3** has only one F substituent at *para* position).

Compound **11** is the only one that has a trifluoromethoxy group instead of a methoxy group. The previous comments apply to **11** except two signals that are slightly out of range, N1 (−110.8 ppm) and C5 (143.3 ppm); these atoms are those closer to the OCF_3 substituent. The ^{13}C of the CF_3 group shows a ^1J SSCC of 256.5 Hz (Table 3).

The NMR data obtained in the solid state are summarized in Tables 4, 6, and 8, where the splitting of some signals is being one of the more interesting results. In ^{13}C cross-polarization magic angle spinning (CPMAS) (Table 4), the C4″ atom of Compound **10** appears at 116.9 and 118.5 ppm that could correspond to two conformations of the methoxy group, **c** and **d** (see below). In ^{15}N CPMAS (Table 6), the N1 signal of Compound **5** is split in two signals at −108.8 and −112.9 ppm ($\Delta\delta = 4.1$ ppm) of the same intensity, and the same occurs for the signal assigned to N4 of Compound **10**, −240.4 and −242.5 ppm ($\Delta\delta = 2.1$ ppm); their origin is uncertain. They could be due to the presence of different independent molecules in the crystal or to through-space dipolar couplings with ^{19}F. In ^{19}F MAS (Table 8), the *ortho*-fluorine atoms (2′ and 6′) appear different due to the absence of rotation of the *N*-aryl ring; the differences are 2.1, 3.7, and 4.8 ppm, for **5**, **8**, and **10**. According to the calculations, the signal appearing at low frequencies corresponds to the F atom

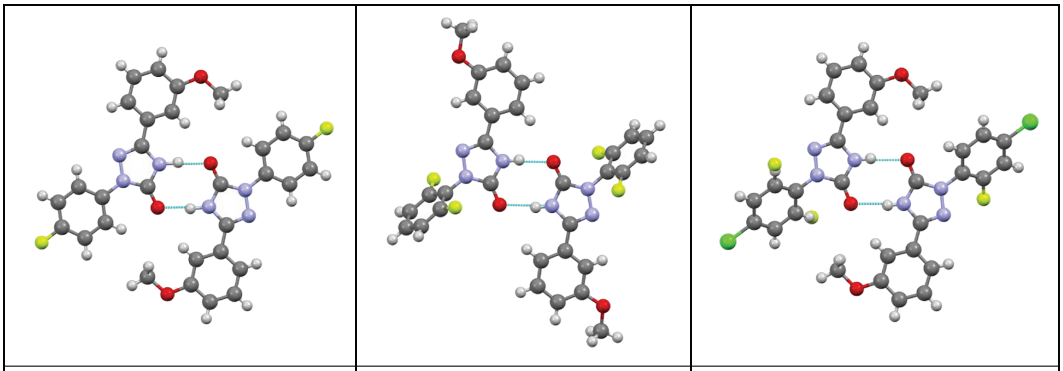

FIGURE 2 The N–H···O═C dimers present in Compounds **3**, **5**, and **6**

FIGURE 3 View of the molecular packing in **3**

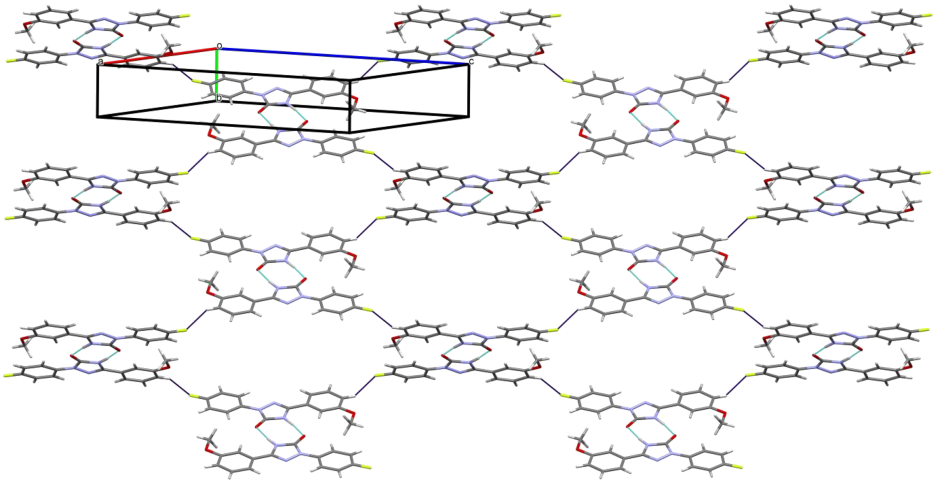

FIGURE 4 View of the molecular packing in **6**

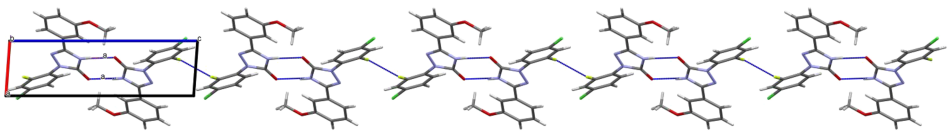

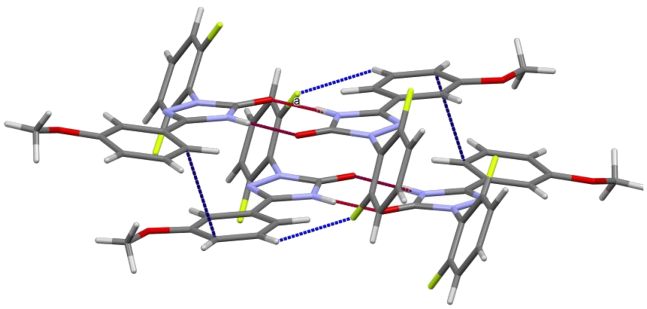

FIGURE 5 View of the molecular packing in **5**

facing the carbonyl group, and that appearing at high frequency corresponds to the F atom near N1; the calculated differences are 1.0, 0.7, and 2.4 ppm, for **5**, **8**, and **10**, respectively.

To compare chemical shifts in solution with those obtained in the solid state, it is necessary to consider that in DMSO solution, the primary and secondary amides form strong HBs with the solvent preventing the formation of intermolecular HBs (rings or chain) that exist in the solid state (see Figure 2). Because the HB is stronger with DMSO than with another solute molecule (as in the crystal), the ^{13}C signal of the C═O group is expected to be shielded ongoing from DMSO solution to solid state; this is what is observed, from 153 to 154–156 ppm, as in the case of 1*H*-pyrrolidone.[25]

Considering the ^{15}N signal of the N4 atom is also involved in HBs, the measured effect going from DMSO solution (−242 ppm) to the compared with the solid state (−240 ppm) is approximately +2 ppm. In the gas phase, it appears at −254 ppm (see Table S2), that is,

deshielded from the condensed phases. Albeit weakly, the solid-state signal appears at a higher frequency than in DMSO compared with the gas phase, +14 and +12 ppm, respectively. In summary, in a first approximation, the conclusion is that DMSO resembles the structure in the solid state for the nuclei studied because in both situations, there is an N–H···O═X HB, where X═S and X═C, respectively.

2.4 | Computational results

2.4.1 | Solution

Conformational analysis

The conformation of the 11 molecules of the present study is related to the torsions about three single bonds:

C3″–O: **a** CX_3 outwards, **b** CX_3 inwards

C5–C1″: **c** OX_3 on the same side than N4–H, **d** OX_3 on the same side than N1

C1′–N2: **e** R on the same side than N1, **f** R on the same side than C3═O. The R substituent can be down (**e** and **f**) or up (**e′** and **f′**).

This results in the 16 rotamers shown in Figure 6.

When the *ortho* positions bear the same substituents (all our *meta* positions have identical substituents, H or F), **e**, **e′**, **f**, and **f′** rotamers are identical, and the number of different conformations is reduced to four. Obviously, there are the 16 corresponding enantiomers that are irrelevant in this paper. If the related dihedral angle is 0° or 90°, the two enantiomers collapse to one; this happens in the X-ray structure of Compound **3** (see previously, Section 2.2) that being completely planar has no enantiomers.

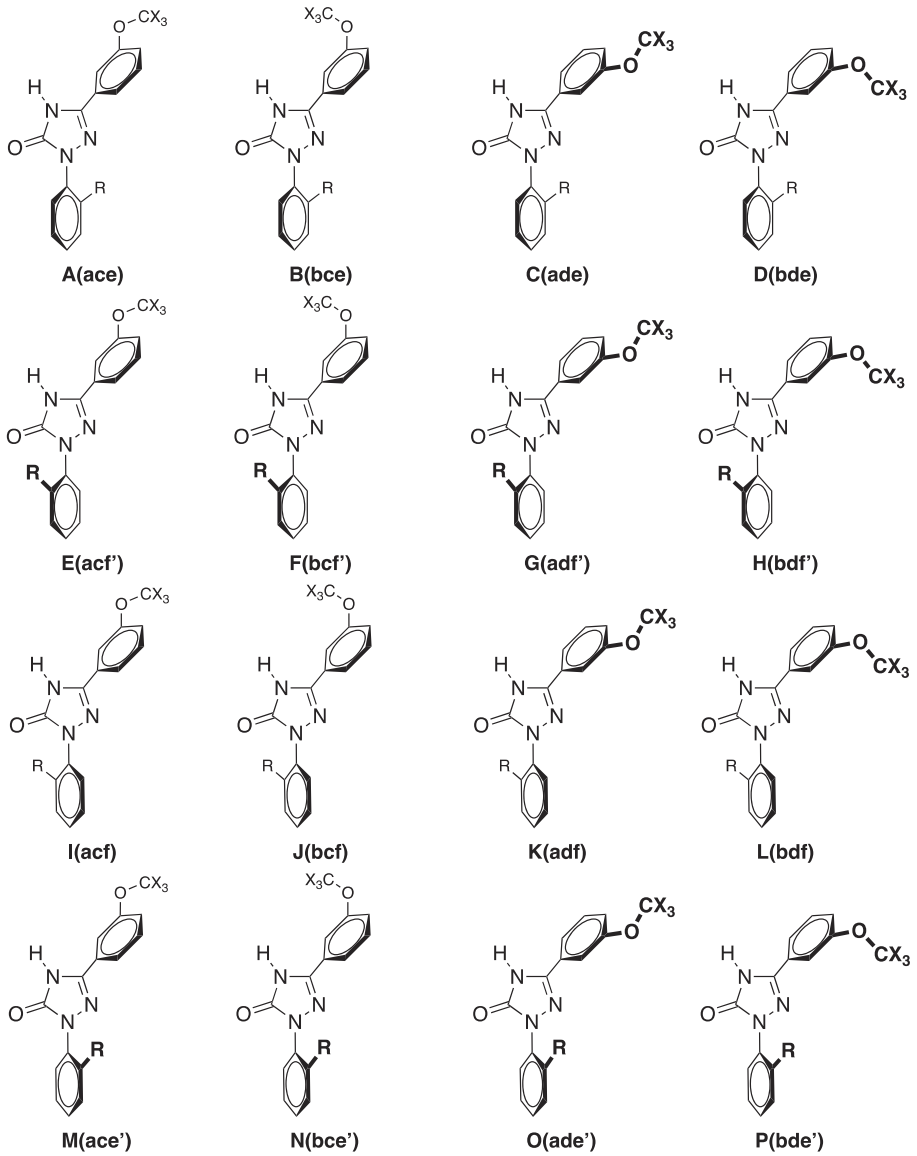

FIGURE 6 The 16 rotamers (X═H or F)

The X-ray structures we have discussed previously correspond to **3═B(bce)═F(bcf)**, **5═C(ade)═G(adf)**, and **6═B(bce)**.

The relative electronic energies of the 16 rotamers of the 11 compounds are reported in Table 9.

There are some coincidences (at 0.1 $kJ{\cdot}mol^{-1}$ precision) because the influence of the torsions upon the *N*-aryl and the *C*-aryl groups on the relative energies are quite independent of each other. Of the three situations present in the 11 compounds, the minima are Compound **1** (2′,4′-dimethyl) **M**; fluorinated derivatives (**2**–**10**) **H** (in Compound **10**, **H** is 0.6 $kJ{\cdot}mol^{-1}$ over **A**), and trifluoromethoxy derivative **11 J**. The mean effects for 16 conformations are reported in the last column of Table 9. This shows that the conformation of the *N*-aryl group (**e**, **e**′, **f**, and **f**′) is not important and that only **a**, **b**, **c**, and **d** determine the stability of the triazolone, in average, 0.5 (**bd**) < 1.6 (**ac**) < 3.1 (**ad**) < 4.7 (**bc**) (Figure 7). It is not possible to go further and obtain the individual (**a**, **b**, **c**, and **d**) contributions because the C5–C1″ (**c**, **d**) and C3″–O (**a**, **b**) conformational effects are not independent but intimately linked; the worse situation corresponds to the CH_3 inwards and the OCH_3 on the same side than N4–H, and the best corresponds to the CH_3 inwards and OCH_3 on the same side than N1.

NMR

The chemical shifts of the isolated molecules that correspond to the gas phase of the 16 conformations for the 11 compounds were calculated excluding both oxygen atoms (C═O and OXH_3) because there are no experimental data. It remains 317 values for which the experimental values were available, except four N atoms, N2 of **2**, N1 of **3**, N2 of **4**, and N1 of **9**.

With the use of the relative energies, we calculated the populations employing the Maxwell–Boltzmann (MB) energy distribution[26] (see the Table S2); then we calculated the absolute shieldings at the GIAO/B3LYP/6-311++G(d,p) level and transformed the absolute shieldings into chemical shifts using robust equations we have reported and frequently used (see Section 3.4).

All the calculated as well as experimental data are given in Table S2. A series of preliminary statistical analyses demonstrated that GIAO's gas phase calculations did not reproduce well four effects: the halogen effect also known as Heavy Atom on Light Atom (HALA) effect of the chlorine atoms on the *ipso* carbons,[27,28] the effect of fluorine atoms on the *ipso* carbons (in previous works we have already noted that the ^{13}C chemical shifts deviate when they bear an fluorine atom),[29] the NH protons that are very sensitive to solvent effects, particularly DMSO, and the N4 atoms that bear the acidic NH proton, which are also sensitive to specific solvent effects, that is, to the N4–H···O═S $(CH_3)_2$ HB.

These four effects were introduced into a data matrix as independent dummy variables (1 if they are present in the atom and 0 if they are absent), in what is called a mixed absence–presence matrix.[28,30–32]

TABLE 9 Relative electronic energies in $kJ{\cdot}mol^{-1}$ of all the minima (in the case of "symmetrical" derivatives, **3**, **5**, **8**, **9**, and **10**, there are only eight different)

	1	2	3	4	5	6	7	8	9	10	11	Mean
A(ace)	2.3	1.9	1.0	1.8	1.5	2.3	2.4	1.1	1.6	**0.0**	2.3	1.4
B(bce)	7.1	5.3	4.1	5.3	3.7	5.4	5.1	3.1	3.9	4.4	1.9	4.7
C(ade)	5.1	3.7	2.4	3.4	2.9	3.8	3.4	2.8	2.7	3.2	0.6	3.3
D(bde)	1.3	0.7	**0.0**	1.0	**0.0**	1.1	0.8	0.0	0.0	0.6	0.8	0.6
E(acf)	3.5	2.2	1.0	2.0	1.5	2.0	1.9	1.1	1.6	**0.0**	0.8	1.7
F(bcf)	7.5	4.7	4.1	4.9	4.2	4.9	4.8	3.1	3.9	4.4	2.7	4.7
G(adf)	4.4	3.6	2.4	3.3	2.9	3.2	3.3	2.8	2.7	3.2	2.7	3.2
H(bdf)	2.7	**0.0**	0.0	**0.0**	0.0	**0.0**	**0.0**	0.0	0.0	0.6	2.0	0.3
I(ace)	4.3	2.2	1.0	2.0	1.5	2.0	1.9	1.1	1.6	**0.0**	2.9	1.8
J(bce)	7.5	4.6	4.1	4.8	3.7	4.8	4.6	3.1	3.9	4.4	**0.0**	4.5
K(ade)	6.2	1.1	2.4	2.2	2.4	2.2	2.5	1.9	2.4	3.2	2.0	2.7
L(bde)	2.9	**0.0**	0.0	**0.0**	0.0	**0.0**	**0.0**	0.0	0.0	0.6	2.7	0.4
M(acf)	**0.0**	1.9	1.0	1.8	1.5	2.3	2.4	1.1	1.6	**0.0**	1.9	1.4
N(bcf)	7.0	5.3	4.1	5.3	3.7	5.5	5.2	3.1	3.9	4.4	2.4	4.8
O(adf)	5.1	3.8	2.4	3.7	2.4	3.9	3.8	1.8	2.4	3.2	0.5	3.3
P(bdf)	1.3	0.7	0.0	1.0	0.0	1.1	0.8	**0.0**	**0.0**	0.6	0.6	0.6

Note: In bold, the minima (0.0); in gray, the identical values due to "symmetry" (**e═f**).

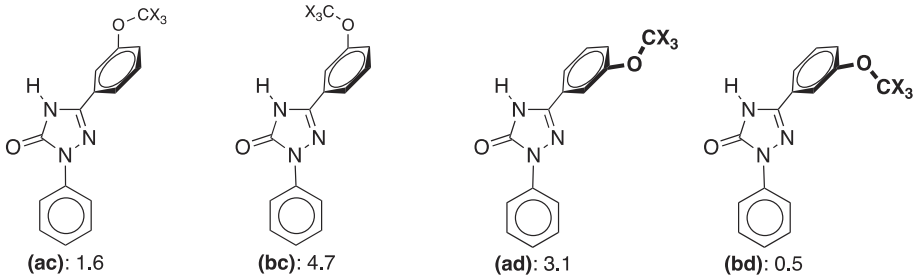

FIGURE 7 The effect of the conformation on the relative electronic energies (in kJ·mol^{-1})

The equation resulting from the comparison of experimental values to those obtained by calculation and MB weighted is

$$\begin{aligned}\text{Exp.} = (1.010 \pm 0.001)\,\text{Calc.} - (10.8 \pm 1.8)^{13}\text{C} - \text{Cl} - (5.0 \pm 0.6)^{13}\\ \text{C} - \text{F} + (14.6 \pm 0.8)^{15}\text{N4} + (5.6 \pm 0.8)^{1}\text{H} - \text{N4},\\ \text{number of observations } 317, R^2 = 0.9995, \text{SE} = 2.6\ \text{ppm}.\end{aligned}$$

This equation allows the calculation of the four missing ^{15}N NMR values:

N2 of **2** (−207.6), N1 of **3**, (−124.6), N2 of **4** (−210.0), and N1 of **9** (−112.0 ppm). In the solid state (Table 6), the corresponding chemical shifts are −204.7, −126.5, −208.9, and −114.6 ppm, in excellent agreement considering the phase effects.

The values in the Tables 3, 4, and 8 marked as "can be permuted" probably by chance agree with the calculated values; that is, small and large chemical shifts are in the correct order.

Our calculations predict that indeed the HALA effect of the chlorine atom, as well as the interaction with the DMSO solvent through the N4–H group, is very significant. The HALA correction for the Cl effect is similar to other values from the literature and from our works.[33–35] For the F atom, we have reported alike values.[29]

Clearly, the effects observed in the N4–H group (+14.6 and 5.6 ppm) are due to the N4–H···O═C3 HB present in the crystal (Figure 2) but not in the monomer. To check this explanation, we have calculated two complexes of Compound **3**, the simplest and most symmetrical triazolone, with DMSO, **3(bc)** and **3(bd)** (Figure 8).

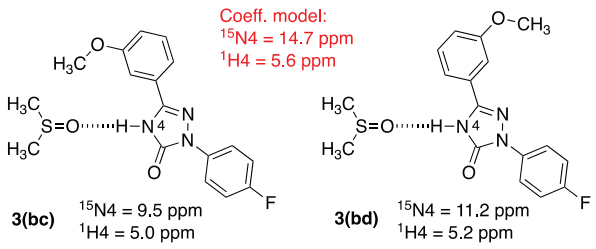

FIGURE 8 The GIAO calculated effects of the DMSO hydrogen bonded to N4–H in Compounds **3(bc)** and **3(bd)**

The agreement is very good especially in the case with **3(bd)B**, the most abundant conformer. The formation of HBs with basic solvents (hydrogen-bond acceptors) shifted the ^{15}N signal of a N–H group 9 ppm (hydrazones, from $CDCl_3$ to DMSO-d_6)[36]; 7–8 ppm (amino-pyrimidines, from CD_3CN to DMSO-d_6)[37]; 10 ppm (pyrrole, from CH_2Cl_2 to DMSO-d_6).[38]

2.4.2 | Solid state

Concerning the solid state, the three compounds that were subjected to X-ray exhibit different space groups, two having a single molecule in the unit cell and one with two molecules in the asymmetric unit. This could have vastly different effects on the SSNMR spectra but as we will see below, this is not the case. The same happens with polymorphism; the Compounds **3**, **5**, and **6** may have polymorphs, but none was found in the present work (no example of polymorphism is known in triazolones). Therefore, we will assume that the crystals we used to determine the X-ray structures and those we used, previously made them a fine powder, corresponds to the same polymorphs.

We have computed the ^{13}C, ^{15}N, and ^{19}F NMR chemical shifts of the Compounds **3**, **5**, and **6** by using the GIPAW method (Table S3).[30,34,39–41] Equations reported in a previous paper[21] were used to transform absolute shielding values (σ, ppm) into chemical shifts (δ, ppm).

A 80:20 disorder of 2′(6′) F atoms in Compound **6** is observed by X-ray but not in ^{19}F SSNMR (Table 8); the same happens in ^{13}C SSNMR for C-2′ (CF) and C-6′ (CH) (Table 4); maybe the minor rotamer is not observed. We solved this disorder aspect by treatment of the crystal structure before theoretical simulation (see computational methods part for technical explanation). The computed ^{19}F NMR chemical shift is −108.5 ppm in agreement with the experimental one (−107.6 ppm). The greatest deviations of the calculated chemical shifts with respect to the experimental values appear in the CO and in N4 atoms, those establishing HBs between the monomers in the unit cell. Remarkably, the C-6′ (**6**) presents the highest

deviation, mostly due to the commented disorder of the fluorine atoms in the crystal structure. Nevertheless, the computed mean absolute error (MAE) is acceptable in all three cases, 3.0 (**3**), 2.7 (**5**), and 2.8 (**6**), indicating that the GIPAW method satisfactorily reproduces the experimental chemical shifts of **3**, **5**, and **6** in solid state.[42]

3 | EXPERIMENTAL

3.1 | Origin of the compounds

The preparation and purification of Compounds **1**–**10** were previously described.[1]

3.1.1 | Synthesis of 2-(2,4-dimethylphenyl)-5-(3-trifluoromethoxyphenyl)-2,4-dihydro-3*H*-1,2,4-triazol-3-one (11)

A mixture of *N*-(aminocarbonyl)-3-(trifluoromethoxy) benzamide (**12**) (1.30 g, 5.24 mmol) and 2,3-dimethylphenylhydrazine (0.71 g, 5.24 mmol) in decalin (16 mL) was stirred at 170°C for 6 h. After cooling, the precipitate was filtered off and washed with diethyl ether (988 mg, 54%): mp 214.0–215.0°C. Anal. Calc. for $C_{17}H_{14}F_3N_3O_2$: C, 58.45; H, 4.04. Found: C, 58.36; H, 4.21%.

3.1.2 | Synthesis of *N*-(aminocarbonyl)-3-(trifluoromethoxy)benzamide (12)

A mixture of 3-(trifluoromethoxy) benzoic acid (2.88 g, 14 mmol, 1 equiv.), 1*H*-benzotriazol-1-yloxytris (dimethylamino)-phosphonium hexafluorophosphate (BOP) (7.28 g, 16.8 mmol, 1.2 equiv.), cyanamide (0.88 g, 21 mmol, 1.5 equiv.), and *N*,*N*-diisopropylethylamine (DIEA) (7.18 mL, 42 mmol, 3 equiv.) in DMF (22.8 mL) was stirred at room temperature for 22 h. 12 N HCl (14 mL) was added, and the reaction mixture was stirred at 50°C for 24 h. After cooling, the precipitate was collected by filtration, washed with water, and vacuum dried to afford Compound **12** as a colorless solid (2.40 g, 69%): mp 182.2–183.2°C; ^{1}H NMR (DMSO-d_6): δ (ppm) 10.71 (br s, 1H, NH), 7.99 (ddd, $^3J_{H5}$ = 7.0 Hz, $^4J_{H2}$ = $^4J_{H4}$ = 1.7 Hz, 1H, H6), 7.95 (br s, 1H, NH_2), 7.91 (br s, 1H, H2), 7.64 (dd, $^3J_{H4}$ = 7.0 Hz, 1H, H5), 7.61 (d, 1H, H4), 7.43 (br s, 1H, NH_2); ^{13}C NMR (DMSO-d_6): δ (ppm) 166.5 ($\underline{CO}NHCONH_2$), 153.9 ($CONH\underline{CO}NH_2$), 148.2 (C3), 134.9 (C1), 130.6 (C5), 127.3 (C6), 125.1 (C4), 120.6 (C2), 120.0 (d, ^1J_F = 257.4 Hz); ^{15}N NMR (DMSO-d_6): δ (ppm) −237.1 (CONHCO), −291.4 ($CONH_2$).

3.2 | X-ray data collection and structure refinement

Data collection for **3**, **5**, and **6** was carried out at room temperature on a Bruker Smart CCD diffractometer using graphite-monochromated Mo-Kα radiation (λ = 0.71073 Å). The diffractometer was operating at 50 kV and 35 mA with an exposure time of 20 s in omega. A summary of the fundamental crystal and refinement data is given in Table S1.

The structures were solved by direct methods and refined by full-matrix least-squares procedures on F^2 using SHELXS and SHELXL programs, respectively,[43] with the aid of the program Olex2.[44] All non-hydrogen atoms were refined anisotropically. The hydrogen atoms were included in their calculated positions and refined as riding on the respective atoms. Atoms H4 linked to N4 atoms were located in a difference Fourier map and refined as riding on the respective bonded atoms.

Compound **5** crystallizes with two molecules in the asymmetric unit. Compound **6** shows a positional disorder for the fluorine atoms over two different positions, which was modeled and refined with occupancies fixed to 80:20.

CCDC 2011717, 2011718, and 2011719 contain the supplementary crystallographic data for this paper. These data can be obtained free of charge from The Cambridge Crystallographic Data Centre via www.ccdc.cam.ac.uk/data_request/cif.

3.3 | NMR experiments

Solution ^{1}H (400.13 MHz), ^{13}C (100.61 MHz), and ^{15}N (40.54 MHz) NMR spectra were recorded on a DRX 400 (9.4 Tesla) spectrometer with a 5-mm inverse-detection H-X probe equipped with a z-gradient coil, regulated at 300 K (27°C). For solution ^{19}F (376.50 MHz) NMR spectra, a 5-mm QNP direct-detection probe equipped with a z-gradient coil was used. Chemical shifts (δ in ppm) are given from internal solvent, DMSO-d_6 2.49 ppm for ^{1}H and 39.5 ppm for ^{13}C, and for ^{15}N and ^{19}F NMR, nitromethane (0.00) and one drop of $CFCl_3$ in $CDCl_3$ (0.00) were used as external references. For ^{13}C and ^{19}F NMR, WALTZ-16 was used for broadband proton decoupling (for ^{19}F NMR, proton coupled spectra were also acquired), and ^{15}N NMR was acquired using 1-D sequence with inverse gated proton decoupling; 2-D

experiments, gs-COSY, gs-HMQC ($^{1}H–^{13}C$), and gs-HMBC ($^{1}H–^{13}C$) were carried out with the standard pulse sequences[45] to assign the ^{1}H and ^{13}C signals.

Solid-state ^{13}C (100.73 MHz) and ^{15}N (40.60 MHz) CPMAS NMR spectra have been obtained on a Bruker WB 400 spectrometer at 300 K using a 4-mm triple channel probehead. Samples were carefully packed in a 4-mm diameter cylindrical zirconia rotor with Kel-F end-caps. ^{13}C spectra were originally referenced to a glycine sample and then the chemical shifts were recalculated to the Me_4Si (for carbonyl atom [glycine] δ = 176.1 ppm) and ^{15}N spectra to $^{15}NH_4Cl$ and then converted to nitromethane scale using the relationship: $\delta^{15}N$(nitromethane) = $\delta^{15}N$(ammonium chloride) – 338.1 ppm. Typical acquisition parameters for ^{13}C CPMAS were 2.9 μs 90° ^{1}H pulses and decoupling field strength of 86.2 kHz by SPINAL 64[46] sequence spectral width, 40 kHz; recycle delay, 5 s; acquisition time, 30 ms; contact time, 2 ms; and spin rate, 12 kHz. In order to distinguish protonated and unprotonated carbon atoms, the Non-Quaternary Suppression (NQS) experiment[47] by conventional cross-polarization was recorded; before the acquisition, the decoupler is switched off for a very short time of 25 μs. Typical acquisition parameters for ^{15}N CPMAS were 2.5-μs ^{1}H 90° pulses (SPINAL 64) spectral width, 40 kHz; recycle delay, 5 s; acquisition time, 35 ms; contact time, 7 ms; and spin rate, 6 kHz.

Solid-state ^{19}F (376.94 MHz) NMR spectra have been obtained on a Bruker WB 400 spectrometer using a MAS DVT BL2.5 X/F/H double resonance probehead. Samples were carefully packed in 2.5-mm diameter cylindrical zirconia rotors with Kel-F end-caps. Samples were spun at the magic angle at rates of 25 kHz, and the experiments were carried out at ambient probe temperature. The typical acquisition parameters $^{19}F\{^{1}H\}$ MAS were spectral width, 75 kHz; recycle delay, 10 s; pulse width, 2.5 μs and proton decoupling field strength of 100 kHz by SPINAL-64 sequence; recycle delay, 10 s; acquisition time, 25 ms; 128 scans; and spin rate, 25 kHz. The ^{19}F spectra were referenced to ammonium trifluoroacetate sample and then the chemical shifts were recalculated to the $CFCl_3$ (δ $CF_3CO_2NH_4^+$ = −72.0 ppm).

3.4 | Computational details

Density functional theory (DFT) calculations were carried out with the Gaussian09 (rev. D.01) suite of programs (Gaussian, Inc., Wallingford, CT, USA).[48] All the conformers (**A**–**P**) of the triazolones **1**–**11** were optimized with the standard B3LYP functional and the 6-311++G(d,p) basis set in the gas phase. The optimizations were carried out using the Berny analytical gradient optimization method.[49] To confirm that the optimized structures were minima or transition states, vibrational frequencies have been calculated at the same level of theory as geometry optimizations, and it was verified that they had only real (minima) or one negative frequency (TS). NMR chemical shifts have been calculated via the "NMR" keyword with the GIAO method[50,51] at the B3LYP/6-311++G(d,p) level of theory in the gas phase and dimethyl sulfoxide.

The following equations[52–54] were used to transform absolute shieldings into chemical shifts:

$$\delta^{1}H = 31.0–0.97 * \sigma^{1}H, \text{ (reference TMS, 0.00 ppm)}$$
$$\delta^{13}C = 175.7–0.963 * \sigma^{13}C, \text{ (reference TMS, 0.00 ppm)}$$
$$\delta^{15}N = -152.0–0.946 * \sigma^{15}N, \text{ (reference } MeNO_2, \text{ 0.00 ppm)}$$
$$\delta^{19}F = 162.1–0.959 * \sigma^{19}F, \text{ (reference } CFCl_3, \text{ 0.00 ppm)}$$

GIPAW method: The geometries of the crystal structures of triazolones **3**, **5**, and **6** were optimized using the generalized gradient approximation (GGA) (Perdew–Burke–Ernzerhof [PBE])[55,56] exchange correlation functional with the Grimme dispersion correction[57,58] and employing the optimization method based on Broyden–Fletcher–Goldfarb–Shanno (BFGS) algorithm and on-the-fly pseudopotentials implemented by default in the CASTEP package. A plane wave kinetic cutoff energy of 900 eV, *k*-point spacing of 0.05 $Å^{-1}$, and ultrafine convergence criteria were applied. Cell parameters remained fixed during the geometry optimization process. These settings were used for the GIPAW calculations of NMR parameters. CASTEP package version 19.1 has been used to run all calculations.[59,60]

These equations were used to transform absolute shielding values (σ, ppm) calculated by the GIPAW method into chemical shifts (δ, ppm):

$$\delta^{13}C = 165.1–0.94 \times \sigma^{13}C$$
$$\delta^{15}N = -160.5–1.08 \times \sigma^{15}N$$
$$\delta^{19}F = 143.0–1.01 \times \sigma^{19}F$$

4 | CONCLUSIONS

In summary, we have reported here a characterization of the tautomeric form and a conformational analysis of 11 2,5-diaryl-4*H*-2,4-dihydro-3*H*-1,2,4-triazol-3-ones, nine

of them bearing fluorine atoms, by NMR, crystallography, and theoretical methods. The ^{13}C, ^{15}N, and ^{19}F NMR chemical shifts in DMSO-d_6 solution are similar to those measured in solid state. The analysis of the most relevant conformers of the triazolones indicates that the presence of OCF_3 instead of OCH_3 reduces the energy difference between them (Table 9). Moreover, the halogen atoms and solvent effects are reflected in the chemical shifts of the ^{13}C and ^{15}N nuclei as revealing their higher coefficients in the computed multiregression through an absence–presence matrix. We have simulated the chemical shifts in solid state of three triazolones whose crystal structures have been resolved in this work, by using the GIPAW methodology with excellent results, including how to treat static disorder problems. Furthermore, our calculations reflect the groups that are interacting by hydrogen bonding and account for the fluorine disorder observed in the X ray diffraction.

ACKNOWLEDGEMENTS

This work was carried out with financial support from the Spanish MICINN for financial support (projects CTQ2018-094644-B-C22 and CTQ2017-87231-P), Comunidad de Madrid (P2018/EMT-4329 AIRTEC-CM), and the Fundación Seneca-CARM (Project 20811/PI/18). Thanks are also given to the CTI (CSIC) for their continued computational support.

ORCID

Marta Marín-Luna https://orcid.org/0000-0003-3531-6622
Pilar Sánchez-Andrada https://orcid.org/0000-0002-9944-8563
Ibon Alkorta https://orcid.org/0000-0001-6876-6211
José Elguero https://orcid.org/0000-0002-9213-6858
M. Carmen Torralba https://orcid.org/0000-0002-2203-1671
Dolores Santa María https://orcid.org/0000-0001-5125-2206
Rosa M. Claramunt https://orcid.org/0000-0001-6634-2677

REFERENCES

[1] D. Santa María, R. M. Claramunt, J. Elguero, M. Carda, E. Falomir, C. Martín-Beltrán, *Med. Chem.* **2019**, *15*, 360.
[2] J. F. Romine, S. W. Martin, V. K. Gribkoff, C. G. Boissard, S. I. Dworetsky, J. Natale, Y. Li, Q. Gao, N. A. Meanwell, J. E. Starrett, *J. Med. Chem.* **2002**, *45*, 2942.
[3] J. Stefanska, M. Struga, S. Tyski, J. Kossakowski, M. Dobosx, *Pol. J. Microbiol.* **2008**, *57*, 179.
[4] N.-B. Sun, J.-Z. Jin, F.-Y. He, *Biomed. Res. Int.* **2015**, *916*, 59.
[5] A. Dorababu, R. R. Kamble, A. A. Kamble, M. N. Kumbar, S. J. Shaikh, S. P. Netalkar, *Chem. Select* **2019**, *4*, 2881.
[6] M. Sharma, S. Garigipati, B. Kundu, D. Vanamala, A. Semwal, D. Sriram, P. Yogeeswari, *Chem. Biol. Drug Res.* **2012**, *80*, 961.
[7] S. Han, F.-F. Zhang, X. Xie, J.-Z. Chen, *Eur. J. Med. Chem.* **2014**, *74*, 73.
[8] M. C. Sharma, S. Sharma, P. Sharma, A. Kumar, K. S. Bhadoriya, *Med. Chem. Res.* **2014**, *23*, 2486.
[9] V. Stoickov, D. Stojanovic, I. Tasik, S. Saric, D. Radenkovic, P. Babovic, D. Sokolovic, A. M. Veselinovic, *Struct. Chem.* **2018**, *29*, 441.
[10] H. Yüksek, E. Koca, O. Gürsoy-Kol, O. Akyildirim, M. Celebier, *J. Mol. Liq.* **2015**, *206*, 359.
[11] R. Xie, X. Mei, J. Ning, *Chem. Pharm. Bull.* **2019**, *67*, 345.
[12] C. F. Tomena, *Prog. Nucl. Magn. Reson.* **2016**, *96*, 73.
[13] R. M. Claramunt, J. L. Lavandera, D. Sanz, M. L. Jimeno, *Tetrahedron* **1998**, *54*, 9569.
[14] *Practical Aspects of Computational Chemistry*, Vol. I, Eds. J. Leszczynski and M. J. Shukla. Chapter 19, O. V. Shishkin, S. V. Shishkina, Unusual properties of usual molecules. Conformational analysis of cyclohexene, its derivatives and heterocyclic analogues. Springer, Dordrecht, **2012**.
[15] I. Alkorta, J. Elguero, C. Roussel, N. Vanthuyne, P. Piras, *Adv. Heterocycl. Chem.* **2012**, *105*, 1.
[16] R. Edwards, J. Madine, L. Fielding, D. A. Middleton, *Phys. Chem. Chem. Phys.* **2010**, *12*, 13999.
[17] I. Alkorta, R. M. Claramunt, E. Díez-Barra, J. Elguero, A. de la Hoz, C. López, *Coord. Chem. Rev.* **2017**, *339*, 153.
[18] M. R. Wormald, A. J. Petrescu, Y.-L. Pao, A. Glithero, T. Elliot, R. Dwek, *Chem. Rev.* **2002**, *102*, 371.
[19] C. I. Nieto, P. Cabildo, M. A. García, R. M. Claramunt, J. Elguero, I. Alkorta, *J. Mol. Struct.* **2017**, *1155*, 205.
[20] M. C. Alvarez-Ros, M. Alcolea Palafox, *Pharmaceuticals* **2014**, *7*, 695.
[21] M. Marín-Luna, I. Alkorta, J. Elguero, *Magn. Reson. Chem.* **2017**, *56*, 164.
[22] J. Elguero, C. Marzin, A. R. Katritzky, P. Linda, *The Tautomerism of Heterocycles*, Academic Press, New York **1976**.
[23] L. Antonov (Ed), *Tautomerism: Concepts and Applications in Science and Technology*, Wiley-VCH, Weinheim **2016**.
[24] S. Berger, S. Braun, H. O. Kalinowski, *NMR Spectroscopy of the Non-Metallic Elements*, Wiley, Chichester **1997**.
[25] S. Molchanov, A. Gryff-Keller, *J. Phys. Chem. A* **2017**, *121*, 9645.
[26] P. W. Atkins, J. de Paula, *Atkins' Physical Chemistry*, 11th ed., Oxford University Press, Oxford **2017**.
[27] L. B. Krivdin, *Prog. NMR Spectrosc.* **2019**, *112–113*, 103.
[28] I. Alkorta, J. Elguero, *Phosphorous Silicon Relat. Elem.* **2020**, *195*, 307.
[29] I. Alkorta, J. Elguero, *Magn. Reson. Chem.* **2019**, *57*, 975.
[30] S. M. Free, J. H. Wilson, *J. Med. Chem.* **1964**, *7*, 395.
[31] J. L. M. Abboud, P. Cabildo, T. Cañada, J. Catalán, R. M. Claramunt, J. L. G. de Paz, J. Elguero, H. Homan, R. Notario, C. Toiron, G. I. Yranzo, *J. Org. Chem.* **1992**, *57*, 3938.
[32] I. Alkorta, J. Elguero, C. Dardonville, F. Reviriego, D. S. María, R. M. Claramunt, M. Marín-Luna, *J. Phys. Org. Chem.* **2020**, *33*, e4042.
[33] A. Wodynski, A. Gryff-Keller, M. Pecul, *J. Chem. Theor. Comp.* **2013**, *9*, 1909.
[34] R. M. Claramunt, C. López, M. A. García, M. D. Otero, M. R. Torres, E. Pinilla, S. H. Alarcón, I. Alkorta, J. Elguero, *New J. Chem.* **2001**, *25*, 1,061.

[35] M. Marín-Luna, R. M. Claramunt, C. I. Nieto, I. Alkorta, J. Elguero, F. Reviriego, *Magn. Reson. Chem.* **2019**, *57*, 275.
[36] R. Marek, A. Lycka, *Curr. Org. Chem.* **2002**, *6*, 35.
[37] E. Kolehmainen, B. Osmialowski, *Int. Rev. Phys. Chem.* **2012**, *31*, 567.
[38] H. Andersson, A.-C. C. Carlsson, B. Nekoueishahraki, U. Brath, M. Erdélyi, *Ann. Rep. NMR Spectrosc.* **2015**, *86*, 73.
[39] A. L. Webber, L. Emsley, R. M. Claramunt, S. P. Brown, *J. Phys. Chem.* **2010**, *114*, 10,435.
[40] M. L. Jimeno, M. T. Benito, E. García Doyagüez, R. M. Claramunt, D. Sanz, M. Marín-Luna, I. Alkorta, J. Elguero, *Magn. Reson. Chem.* **2016**, *54*, 684.
[41] M. Marín-Luna, I. Alkorta, J. Elguero, *Magn. Reson. Chem.* **2018**, *56*, 164.
[42] G. J. O. Beran, J. D. Hartman, Y. N. Heit, *Acc. Chem. Res.* **2016**, *49*, 2,501.
[43] (a) G. M. Sheldrick, *Acta Crystallogr.* **2008**, *A64*, 112. (b) G. M. Sheldrick, *Acta Crystallogr.* **2015**, *C71*, 3.
[44] O. V. Dolomanov, L. J. Bourhis, R. J. Gildea, J. A. K. Howard, H. Puschmann, *J. Appl. Cryst.* **2009**, *42*, 339.
[45] S. Berger, S. Braun, *200 and More NMR Experiments*, Wiley-VCH, Weinheim **2004**.
[46] B. M. Fung, A. K. Khitrin, K. Ermolaev, *J. Magn. Reson.* **2000**, *142*, 97.
[47] R. K. Harris, P. Jonsen, K. J. Packer, *Org. Magn. Reson.* **1984**, *22*, 269.
[48] M. J. Frisch, G. W. Trucks, H. B. Schlegel, G. E. Scuseria, M. A. Robb, J. R. Cheeseman, G. Scalmani, V. Barone, G. A. Petersson, H. Nakatsuji, X. Li, M. Caricato, A. V. Marenich, J. Bloino, B. G. Janesko, R. Gomperts, B. Mennucci, H. P. Hratchian, J. V. Ortiz, A. F. Izmaylov, J. L. Sonnenberg, D. Williams-Young, F. Ding, F. Lipparini, F. Egidi, J. Goings, B. Peng, A. Petrone, T. Henderson, D. Ranasinghe, V. G. Zakrzewski, J. Gao, N. Rega, G. Zheng, W. Liang, M. Hada, M. Ehara, K. Toyota, R. Fukuda, J. Hasegawa, M. Ishida, T. Nakajima, Y. Honda, O. Kitao, H. Nakai, T. Vreven, K. Throssell, J. A. Montgomery Jr., J. E. Peralta, F. Ogliaro, M. J. Bearpark, J. J. Heyd, E. N. Brothers, K. N. Kudin, V. N. Staroverov, T. A. Keith, R. Kobayashi, J. Normand, K. Raghavachari, A. P. Rendell, J. C. Burant, S. S. Iyengar, J. Tomasi, M. Cossi, J. M. Millam, M. Klene, C. Adamo, R. Cammi, J. W. Ochterski, R. L. Martin, K. Morokuma, O. Farkas, J. B. Foresman, D. J. Fox, *Gaussian 16, Revision A.03*, Gaussian, Inc, Wallingford CT **2016**.
[49] H. B. Schlegel, *J. Comput. Chem.* **1982**, *3*, 214.
[50] F. London, *J. Phys. Radium* **1937**, *8*, 397.
[51] R. Ditchfield, *Mol. Phys.* **1974**, *27*, 789.
[52] A. M. S. Silva, R. M. S. Sousa, M. L. Jimeno, F. Blanco, I. Alkorta, J. Elguero, *Magn. Reson. Chem.* **2008**, *46*, 859.
[53] F. Blanco, I. Alkorta, J. Elguero, *Magn. Reson. Chem.* **2007**, *45*, 797.
[54] N. Fresno, R. Pérez-Fernández, M. L. Jimeno, I. Alkorta, G. Sánchez-Sanz, J. Elguero, J. E. Del Bene, *J. Heterocyclic Chem.* **2012**, *49*, 1257.
[55] J. P. Perdew, K. Burke, Y. Wang, *Phys. Rev. B* **1996**, *54*, 16533.
[56] J. P. Perdew, K. Burke, M. Ernzerhof, *Phys. Rev. Lett.* **1996**, *77*, 3865.
[57] S. Grimme, *J. Comput. Chem.* **2004**, *25*, 1463.
[58] S. Grimme, *J. Comput. Chem.* **2006**, *27*, 1787.
[59] S. J. Clark, M. D. Segall, C. J. Pickard, P. J. Hasnip, M. J. Probert, K. Refson, M. C. Payne, *Z. Kristallogr.* **2005**, *220*, 567.
[60] M. D. Segall, P. J. D. Lindan, M. J. Probert, C. J. Pickard, P. J. Hasnip, S. J. Clark, M. C. Payne, *J. Phys. Condens. Matter* **2002**, *14*, 2717.

SUPPORTING INFORMATION

Additional supporting information may be found online in the Supporting Information section at the end of this article.

How to cite this article: Marín-Luna M, Sánchez-Andrada P, Alkorta I, et al. A structural analysis of 2,5-diaryl-4*H*-2,4-dihydro-3*H*-1,2,4-triazol-3-ones: NMR in the solid state, X-ray crystallography, and GIPAW calculations. *Magn Reson Chem*. 2021;59:423–438. https://doi.org/10.1002/mrc.5107